

A Data-Driven Forced Oscillation Locating Method for Power Systems with Inverter-Based Resources

Yaojie Cai, Georgia Pierrou, *Member, IEEE*, Xiaozhe Wang, *Senior Member, IEEE*, and Geza Joos, *Life Fellow, IEEE*

Abstract—Forced Oscillations (FO) stemming from external periodic disturbances threaten power system security and stability. The increasing penetration of Inverter-Based Resources (IBRs) further introduces FO, leading to new challenges in identifying and locating FO sources in modern power systems. In this paper, a novel data-driven method for locating FO in power systems with IBRs is proposed. Unlike previous works, a unified representation of FO originating from IBRs is considered, which further facilitates the development of the FO locating algorithm. Leveraging on Sparse Identification for a Nonlinear Dynamical (SINDy), a purely data-driven methodology is developed for locating the source of FO by interpreting the proposed model from measurements. Numerical results on the WECC 240-bus system validate the performance of the proposed approach in successfully locating FO in the presence of IBRs.

Index Terms—forced oscillations, low frequency oscillations, inverter-based resources (IBRs), Sparse Identification of Nonlinear Dynamics (SINDy)

I. INTRODUCTION

Forced Oscillations (FO), i.e., oscillations that may appear due to external periodic disturbances, pose a significant threat to the security and stability of electric power systems. Relevant studies have mostly focused on FO introduced by synchronous generators, for instance, in cases where a periodic forcing is imposed on the generator shaft due to inappropriate parameters in the control loop from turbine governor or exciter.

In recent years, real life events indicate that FO may also originate from Inverter-Based Resources (IBRs). In fact, it has been shown in [1] that abnormal renewable generator operating conditions, such as wind shear and solar irradiance changes, may lead to FO. Besides, when the FO frequency is low and close to the system modes, it can create resonance conditions with significant oscillations occurring far from the source. More such events have been observed with the increasing deployment of IBRs [2], highlighting the need to identify FO sources originating from converter stations. Consequently, it is of paramount importance that FO are properly identified and their source is located in power systems with both conventional generation and IBRs.

One approach to locating the source of FO is the Dissipating Energy Flow (DEF) method, which identifies the bus with the highest positive DEF among generation buses as the FO source [3]. Although effective in many scenarios, DEF struggles with oscillations from synchronous generator excitation control [4]. To address this, the Complex Dissipating Energy Flow (CDEF)

method was proposed [5], introducing a path-dependent energy function that incorporates line conductance and bus voltage changes, significantly improving DEF's accuracy. In addition, it is tested in [6] that DEF can be used in the presence of converter-based generation if the complex energy flow is calculated using D-Q axis measurements. However, both DEF and CDEF methods assume that lines are lossless, which may not be practical. Indeed, it has been shown in [7] that the DEF method might become less effective when calculating the DEF through lossy transmission lines.

To locate the source of the FO with minimal assumptions, machine learning-based approaches [8]–[12] have been widely applied. K-nearest neighbours classification [8] and deep transfer learning algorithm [12] show promising results in numerical studies. However, the aforementioned methods require a large amount of training data and retraining is needed before deployment to a new system. Apart from locating the source using blackbox network equations, several methods focus on dynamic components, assuming the system can be represented as low-rank using measurement data. The authors in [10] show that FO can be analyzed with a low-rank foreground matrix representing system modes and a sparse background matrix for the corresponding forced input. However, when dealing with a large-scale power system, the size of the matrix and consequently the computational demands can rise sharply. In [11], the Sparse Identification of Nonlinear Dynamics (SINDy) methodology introduced by [13] is utilized to develop a FO locating method in a system with synchronous generators. Yet, locating FO originating from IBRs is not modeled or considered.

To study FO in systems with IBRs, [14] extends the swing equation that describes synchronous generation dynamics for representing wind power. Nevertheless, the swing equation cannot capture the dynamics of IBRs, as they do not have rotating masses and only interact with the grid through different electronic controls. Thus, a unified model that reflects the convector control characteristics is missing. Another promising methodology that utilizes the Variational Mode Decomposition (VMD) and Cross-Power Spectral Density (CPSD) is presented in [15]. Although FO originating from High Voltage Direct Current (HVDC) systems are included, further testing is needed to assess the effectiveness of the VMD-CPSD method in identifying FO from IBRs.

To address the aforementioned issues, this paper presents a novel data-driven method for locating FO in power systems with IBRs. Different from [11] that focuses solely on FO from synchronous generators, this work integrates the presence of

This work was supported in part by the Fonds de recherche du Québec – Nature et technologies (FRQNT) under Grant 256837 and 259083, and in part by the Natural Sciences and Engineering Research Council of Canada (NSERC) under Discovery Grant RGPIN-2022-03236

IBR devices, such as HVDC and renewable generation, that can also lead to FO. In particular, a unified representation of a converter model for FO studies based on Phase-Locked Loop (PLL) dynamics is considered, which facilitates having a common formulation of FO originating from various grid-following (GFL) IBRs. By utilizing SINDy, the sources of FO can be identified by extracting the model coefficients from measurements. The effectiveness of the proposed method has been validated through a comprehensive numerical study conducted on the WECC 240-bus system [16], including scenarios of FO originating from HVDC converter stations and renewable generation converters. In sum, the main contributions of this paper are presented below:

- 1) A unified representation for FO sourced from GFL IBRs is proposed, allowing for the development of a data-driven FO locating algorithm for systems with both synchronous generators and GFL IBRs.
- 2) An extended SINDy function library is designed to effectively integrate GFL IBRs as potential FO sources.
- 3) The proposed method is purely data-driven and requires no additional dynamic model or network parameters.
- 4) Comparisons of the proposed approach with respect to state-of-the-art methods are performed on the WECC 240 bus system, which further illustrates the effectiveness of the proposed approach under resonance conditions and non-stationary FO of multiple frequencies.

The remainder of the paper is organized as follows: Section II reviews the preliminaries regarding the dynamic model and FO study in the case of synchronous generators, Section III describes the FO mechanisms from GFL IBRs. Section IV describes the proposed FO locating method. Section V presents case studies for validation. Section VI summarizes the conclusions and perspectives for future work.

II. PRELIMINARIES

A. Dynamic Model of Synchronous Generator

The classical synchronous generator model (i.e., the swing equation) is considered in this study as we are interested in system dynamics in ambient conditions. In particular, the equations which govern generator rotor angles and speed deviations due to stochastic load variations can be expressed as [17], [18]:

$$\begin{aligned} \dot{\delta} &= \omega \\ M\dot{\omega} &= P_m - P_e - D\omega - \Sigma\eta \end{aligned} \quad (1)$$

where $\delta = [\delta_1, \dots, \delta_\iota]^T$ is the vector of rotor angles, $\omega = [\omega_1, \dots, \omega_\iota]^T$ is the vector of rotor speed deviations from the synchronous speed, $P_e = [P_{e_1}, \dots, P_{e_\iota}]^T$ denotes the vector of electrical power outputs, $P_m = [P_{m_1}, \dots, P_{m_\iota}]^T$ denotes the vector of mechanical power inputs, and $D = \text{diag}[D_1, \dots, D_\iota]$ is the matrix that includes the damping coefficients. In addition, $\eta = [\eta_1, \dots, \eta_\iota]^T$ is a standard Gaussian random vector and $\Sigma = \text{diag}[\sigma_1, \dots, \sigma_\iota]$ represents the corresponding standard deviations that describe the load power variations reflected on the generation side.

In FO study, an input $u_{\omega F}$ may represent the periodic forcing imposed on the generator turbine shafts and therefore

mechanical power P_m due to, for example, oscillatory load, mistuned control parameters, or malfunction equipment [1]. Thus, the dynamic model of synchronous generators under FO can be represented as:

$$\begin{bmatrix} \Delta\dot{\delta} \\ \Delta\dot{\omega} \end{bmatrix} = \begin{bmatrix} 0_{\iota \times \iota} & I_{\iota \times \iota} \\ -M^{-1}\frac{\partial P_e}{\partial \delta} & -M^{-1}D \end{bmatrix} \begin{bmatrix} \Delta\delta \\ \Delta\omega \end{bmatrix} - \begin{bmatrix} 0_{\iota \times 1} \\ M^{-1}\Sigma\eta \end{bmatrix} + [u_{\omega F}] \quad (2)$$

where Δ denotes the difference between the currently measured and the steady state value, and $u_{\omega F}$ can be represented as:

$$u_{\omega F} = \sum_{i=1}^l \left(\begin{bmatrix} a_{\delta_i} \\ a_{\omega_i} \end{bmatrix} \sin(\omega_{F_i} t) + \begin{bmatrix} b_{\delta_i} \\ b_{\omega_i} \end{bmatrix} \cos(\omega_{F_i} t) \right) \quad (3)$$

where $a_{\delta_i}, a_{\omega_i}, b_{\delta_i}, b_{\omega_i}$ are $\iota \times 1$ vectors that include the coefficients describing the magnitudes of each generator's input at the corresponding frequency $\omega_{F_i}, i = 1, \dots, l$. As discussed in our previous work [11], FO generated by excitation systems, including exciters, Power System Stabilizers (PSSs), and turbine governors, will manifest themselves in rotor dynamics. Therefore, the model is sufficient to capture FO sourced from synchronous generators.

B. Forced Oscillation Locating Method for Systems with Synchronous Generators

Looking at (2), it can be observed that in case the system has a single FO source, the corresponding state with a small amount of trigonometric function coefficients is non-zero. It has been shown in [11] that locating the FO in the context of power systems when the FO source is a synchronous generator can be achieved by leveraging on measurements and SINDy developed by Brunton et al. in [13]. Let $x = [\Delta\delta^T, \Delta\omega^T]^T$, and X contains τ_ω snapshots of the state variable x and takes the form $X = [x_1, \dots, x_{\tau_\omega}]^T$. Briefly, the system (2) can be written in the SINDy form as:

$$\dot{X} = \Xi\Theta^T(X) \quad (4)$$

where the coefficient matrix Ξ and the feature library $\Theta(X)$ are given as:

$$\Xi = \begin{bmatrix} \Xi_\eta & \Xi_{\text{Jacobian}} & \Xi_{ab} \end{bmatrix} \quad (5)$$

$$\Xi_\eta = \begin{bmatrix} 0 \\ -M^{-1}E^2G\Sigma\eta \end{bmatrix} \quad (6)$$

$$\Xi_{\text{Jacobian}} = \begin{bmatrix} 0 & I \\ -M^{-1}\frac{\partial P_e}{\partial \delta} & -M^{-1}D \end{bmatrix} \quad (7)$$

$$\Xi_{ab} = \begin{bmatrix} | & | & \dots & | & | \\ a_{\delta_1} & b_{\delta_1} & \dots & a_{\delta_\iota} & b_{\delta_\iota} \\ | & | & \dots & | & | \\ a_{\omega_1} & b_{\omega_1} & \dots & a_{\omega_\iota} & b_{\omega_\iota} \\ | & | & \dots & | & | \end{bmatrix} \quad (8)$$

$$\Theta^T(X) = \begin{bmatrix} - & 1 & - \\ & X & \\ - & \sin(\omega_{F_1} t) & - \\ - & \cos(\omega_{F_1} t) & - \\ \vdots & \vdots & \vdots \\ - & \sin(\omega_{F_l} t) & - \\ - & \cos(\omega_{F_l} t) & - \end{bmatrix} \quad (9)$$

Yet, in practice, the success of the source-locating algorithm depends on the sufficient and reasonable feature terms in the SINDy function library. The classic generator model used in [11] cannot accurately represent modern power systems with integrated IBR devices, such as HVDC and renewable generation sources, which include GFL control and are decoupled from machine dynamics through a DC link. A common dynamic model is needed to allow [11] to further locate the FO source from a GFL IBR device with an unknown control loop structure. Thus, in the next sections, this paper proposes a general set of dynamic governing equations for locating different FO in power systems, originating from either conventional synchronous generators or inverter-based renewable generation and the converter control.

III. FORCED OSCILLATION MECHANISMS FROM INVERTER-BASED RESOURCES

A. Dynamic Model of Grid-Following Inverter-Based Resources

The generalized angle dynamics for GFL IBRs [19] demonstrate that the dynamics of the PLL are a major contributor to the overall angle dynamics and are implemented in most grid-following IBRs. A standard synchronous reference frame PLL with a proportional-integral (PI) controller (PI-PLL) [19] is illustrated in Fig. 1. In particular, the Q-axis component v_q is derived from the three-phase AC voltage at the Common Coupling Point (CCP) V_{ccp} by applying Park's transformation. A PI controller with proportional and integral gains, K_{PLLp} and K_{PLLI} , is employed for low-pass filtering whereas ω_g represents the system's nominal frequency.

Thus, the PLL equation for the dynamics of the angle θ can be described as:

$$\dot{\theta} = K_{PLLp} v_q + K_{PLLI} \int v_q \quad (10)$$

Assuming the system is connected with r IBR devices, (10) can be linearized and written in a compact form as follows:

$$[\Delta \dot{\theta}]_{r \times 1} = [K_{PLLp} \times I \quad K_{PLLI} \times I]_{r \times 2r} \begin{bmatrix} \Delta v_q \\ \Delta v_{qI} \end{bmatrix}_{2r \times 1} \quad (11)$$

where θ, v_q, v_{qI} are vectors that include the angles and the corresponding voltage components and I is the identity matrix. Specifically, as illustrated in Fig. 1, v_{qI} is obtained by v_q after applying the integral gain.

Next, various FO mechanisms from GFL IBRs documented in previous literature will be discussed, examining their origins, characteristics, and impacts on system dynamics. Despite the diversity of IBR-related mechanisms causing FO, we will show that they can consistently be represented as disturbances injected into V_{ccp} as:

$$V_{ccpFO} = V_{ccp} + u_F \quad (12)$$

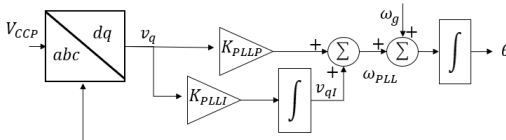


Fig. 1: PI Control-based PLL block diagram.

where V_{ccpFO} denotes the AC voltage under FO and u_F is the disturbance injected in V_{ccp} due to FO. This unified representation allows for the development of a data-driven FO locating algorithm for power systems with GFL IBRs, as will be shown in Section IV.

B. Forced Oscillation from Wind Generation

The periodic fluctuation of wind becomes a potential source of FO. If the equivalent wind speed v_{eqws} under wind shear and tower shadow is the source of the injection of FO, it can be represented as [20]:

$$v_{eqws} = v_{eq} + v_{F,wind} \quad (13)$$

where v_{eq} is the hub-height wind speed and $v_{F,wind}$ is the disturbance observed in the wind speed. The wind speed variation will be reflected in the power harvested by the turbine P_{windFO} as follows:

$$P_{windFO} = \frac{1}{2} \rho A_{swept} v_{eqws}^3 C_p \quad (14)$$

where ρ is the air density, A_{swept} is the swept area of the turbine blade, and C_p is the power coefficient [21]. Hence, if v_{eqws} varies periodically, oscillations will be observed in wind generated power. It is worth noting that it has been shown in [22] that the frequency range for low-order oscillations induced from wind turbine control schemes is 0.388 to 0.775 Hz.

C. Forced Oscillation from Solar Generation

In addition, periodic fluctuations in solar irradiance can cause FO in solar power injection. Event 22 in [1] reports a forced oscillation event associated with rapid changes in solar irradiance. Similarly, [23] shows that sudden increases in irradiance due to cloud edge reflection, particularly under weak grid conditions, can interact with inverter control systems and potentially induce oscillations. Furthermore, [24] reports significant irradiance variability due to cloud cover in southern Norway and highlights that such fluctuations that occur in seconds to minutes can affect power quality, leading to voltage dips, flicker, and even frequency oscillations. [25], [26] analyze power output data from a PV plant, demonstrating that transient clouds whose speed and size influence the duration of shading events result in power oscillations around 4 Hz. Consequently, similar to the case of the wind speed, the varying solar irradiance g_{eqirr} can be assumed as an equivalent irradiance g_{eq} with a periodic signal injection $g_{F,irr}$ [27]:

$$g_{eqirr} = g_{eq} + g_{F,irr} \quad (15)$$

As a result, the generated solar power $P_{solarFO}$ is affected as follows:

$$P_{solarFO} = A_{panel} C_{solar} g_{eq,irr} \quad (16)$$

where A_{panel} is the area and C_{solar} is the efficiency of the solar panel.

In sum, (14) and (16) demonstrate that FO originating from either wind generators or variations in solar irradiance will be manifested as oscillations in power injections, i.e., P_{meas} in Fig. 2. Consequently, as indicated by the simplified

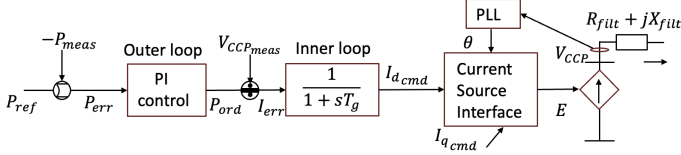


Fig. 2: Simplified converter control block diagram.

converter control block diagram in Fig. 2, these oscillations will also appear in the measured voltages at the CCP. To further illustrate that, Fig. 3 depicts simulation results in the WECC 240-bus system [16], where oscillations in both the magnitude and angle of the voltage V_{ccp} are observed once a sinusoidal signal is injected to the active power reference of a solar converter.

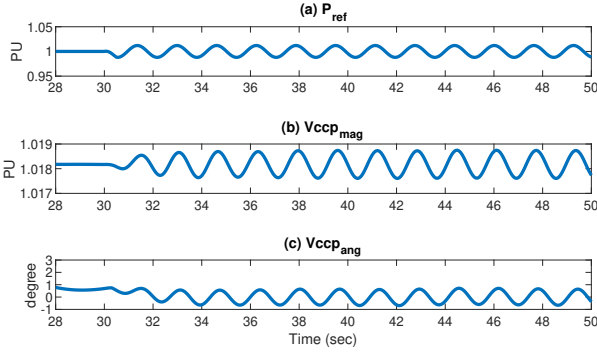


Fig. 3: (a) Active power reference (b) V_{ccp} magnitude (c) V_{ccp} angle under FO by solar in the WECC 240-bus system.

D. Forced Oscillation from Converter Control

Except for the inherent uncertain characteristics of the wind speed and solar irradiance, many real-world events indicate that IBR devices can also experience FO due to malfunctioning controllers [1]. Indeed, previous works (e.g., [28], [29]) demonstrate that incorrect parameter settings in various control strategies can lead to undesirable periodic signals in V_{ccp} when system operating conditions change, such as during power ramping or fault occurrences.

More specifically, [30] shows that the high PLL gain selection for a converter in a poor grid condition may lead to fast, aggressive responses and eventually oscillatory behaviour in V_{ccp} . When the IBR shuts down because of overvoltage, [29] shows that the wrong hysteresis function (determined by a trial-and-error strategy) in the curtailment ON-OFF control can result in the voltage falling below the turn-on value, causing the unit to repeat the stop and restart process and producing an unwanted sawtooth wave at V_{ccp} . Furthermore, [31], [32] show that long time delays due to analog-to-digital conversions or communication of the control loop actions may result in oscillations in V_{ccp} . In addition, paper [28] identifies that oscillations of very low frequency (around 0.1 Hz) may appear in V_{ccp} when PV power plants ramp up real power due to communication delays in the volt-var control.

As further shown in [16], injecting a sinusoidal signal into the DC voltage control of an HVDC sending end converter

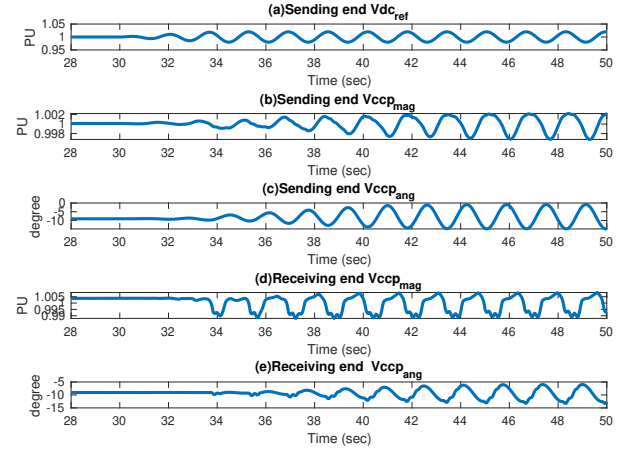


Fig. 4: (a) DC voltage reference, sending end (b and c) and receiving end (d and e) V_{ccp} magnitude and V_{ccp} angle under FO by HVDC control in the WECC 240-bus system.

causes both the magnitude and phase of sending and receiving end V_{ccp} to oscillate. To further demonstrate this, Fig. 4 presents relevant simulation results obtained from the WECC 240-bus system where a FO signal is injected at the DC voltage reference of the sending end bus of the HVDC link. Therefore, as proposed by (12), we will model the oscillations caused by the mistuning of IBR converter control as injected signals into the CCP voltage. Lastly, it is important to note that FO can occur across a broad frequency range. However, this study focuses specifically on low-frequency FO, as these can overlap with the system's natural modes, making source identification particularly challenging.

IV. SINDY-BASED FORCED OSCILLATION LOCATING METHOD WITH GRID-FOLLOWING INVERTER-BASED RESOURCES

A. Dynamic Model of Systems with Grid-Following Inverter-Based Resources under Forced Oscillations

As discussed in the previous section, FO from IBRs will show up at V_{ccp} . Since v_q is obtained by applying Park's transformation to V_{ccp} , the FO will also appear at v_q , which is the input to PLL dynamics as demonstrated by (11). Thus, for r IBR devices, if \mathbf{u}_F is sourced from IBRs, it can be termed as forcing sine and cosine signals added to v_q and its numerical integration v_{qI} in (11) as below:

$$\begin{aligned} [\Delta \dot{\theta}] &= [K_{PLL P} \times I \quad K_{PLL I} \times I]_{r \times 2r} \\ &\times \left(\begin{bmatrix} \Delta v_q \\ \Delta v_{qI} \end{bmatrix}_{2r \times 1} + \mathbf{u}_F \right) \\ &= [K_{PLL P} \times I \quad K_{PLL I} \times I] \begin{bmatrix} \Delta v_q \\ \Delta v_{qI} \end{bmatrix} + \\ &\sum_{i=1}^l (A_{IBR_i} \sin(\omega_{F_i} t) + B_{IBR_i} \cos(\omega_{F_i} t)) \end{aligned} \quad (17)$$

A_{IBR_i} , B_{IBR_i} are vectors describing each IBR's contribution to each ω_{F_i} , $i = 1, \dots, l$. Specifically,

$$A_{IBR_i} = [K_{PLL P} \times I \quad K_{PLL I} \times I] \begin{bmatrix} a_{v_q i} \\ a_{v_{qI} i} \end{bmatrix} \quad (18)$$

and

$$B_{IBR_i} = \begin{bmatrix} K_{PLLP} \times I & K_{PLLI} \times I \end{bmatrix} \begin{bmatrix} b_{v_q i} \\ b_{v_{qI} i} \end{bmatrix} \quad (19)$$

where $a_{v_q i} = [a_{v_q i_1}, \dots, a_{v_q i_r}]^T$, $a_{v_{qI} i} = [a_{v_{qI} i_1}, \dots, a_{v_{qI} i_r}]^T$, $b_{v_q i} = [b_{v_q i_1}, \dots, b_{v_q i_r}]^T$, and $b_{v_{qI} i} = [b_{v_{qI} i_1}, \dots, b_{v_{qI} i_r}]^T$ are $r \times 1$ vectors that include the coefficients of the IBRs for the corresponding frequency ω_{F_i} .

B. Forced Oscillation Locating

The full set of dynamic equations for the bulk power system during FO events incorporates the dynamics of synchronous machines in (2) along with the ones of GFL IBRs in (17). Thus, the complete model can be expressed in the form of (4) as follows, which can be identified using SINDy:

$$\begin{bmatrix} \Delta \dot{\delta} \\ \Delta \dot{\theta} \\ \Delta \dot{\omega} \end{bmatrix} = \Xi \Theta^T(X) = \Xi \begin{bmatrix} 1 \\ \Delta \delta \\ \Delta \omega \\ \Delta v_q \\ \Delta v_{qI} \\ \sin(\omega_{F_1} t) \\ \cos(\omega_{F_1} t) \\ \vdots \\ \sin(\omega_{F_l} t) \\ \cos(\omega_{F_l} t) \end{bmatrix} \quad (20)$$

and

$$\Xi^T = \begin{bmatrix} 0 & 0 & (-M^{-1}\Sigma\eta)^T \\ 0 & 0 & (-M^{-1}\frac{\partial P_e}{\partial \delta})^T \\ I & 0 & (-M^{-1}D)^T \\ 0 & K_{PLLP} \times I & 0 \\ 0 & K_{PLLI} \times I & 0 \\ a_{\delta_1}^T & A_{IBR_1}^T & a_{\omega_1}^T \\ b_{\delta_1}^T & B_{IBR_1}^T & b_{\omega_1}^T \\ \vdots & \vdots & \vdots \\ a_{\delta_l}^T & A_{IBR_l}^T & a_{\omega_l}^T \\ b_{\delta_l}^T & B_{IBR_l}^T & b_{\omega_l}^T \end{bmatrix} \quad (21)$$

where a_{ω_i} , b_{ω_i} , a_{δ_i} , b_{δ_i} , A_{IBR_i} and B_{IBR_i} include the coefficients associated with the sinusoidal terms as introduced in (3), (17). Note that $\Delta \delta$ and $\Delta \omega$ are the deviations of the rotor angles and rotor speeds of synchronous generators, respectively, and $\Delta \theta$ are the deviations of IBRs PLL angles.

Recall the SINDy form from Section II, the X matrix on the left-hand side of (20) can be built by using either directly obtained or calculated from PMU measurements associated with the state variables of synchronous generators and GFL IBR devices with a window size τ_ω . Let $x = [\Delta \delta^T, \Delta \theta^T, \Delta \omega^T]^T$, and X contains τ_ω snapshots of the state variable x :

$$X = \begin{bmatrix} | & | & \dots & | \\ x_1 & x_2 & \dots & x_{\tau_\omega} \\ | & | & \dots & | \end{bmatrix} \quad (22)$$

In addition, the right-hand side library matrix $\Theta(X)$ of (20) is built as:

$$\Theta(X) = \begin{bmatrix} | & \dots & | & \dots & | & \dots & | & \dots \\ 1 & \dots & \Delta \delta_l & \dots & \Delta \omega_l & \dots & \Delta v_{q_r} & \dots \\ | & \dots & | & \dots & | & \dots & | & \dots \end{bmatrix} \quad (23)$$

$$\begin{bmatrix} | & \dots & | & \dots & | \\ \Delta v_{qI_r} & \dots & \sin(\omega_{F_i} t) & \dots & \cos(\omega_{F_i} t) \\ | & \dots & | & \dots & | \end{bmatrix}$$

Each column in $\Theta(X)$ means τ_ω snapshots of the variable. The data for the integral control v_{qI} can be calculated discretely with the time step, a data buffer record, and numerical integration using the trapezoid or Simpson's rule (24) [33] as:

$$v_{qI} = \int_{t-\tau}^t v_q dt = \frac{\tau}{2} [v_q(t) + v_q(t-\tau)] \quad (24)$$

where τ is the time step of the measurements.

Next, the Fast Fourier Transform (FFT) is applied to the magnitude and phase angle of each element of V_{cep} . By rescaling the maximum amplitude of the spectrum from FFT between 0 and 1, the FO frequencies can be obtained through a z-score-based peak detection method [34] with a threshold of 1 from the resulting spectrum for each measurement. Up to three ($l \leq 3$) potential frequencies are selected from the spectrum, assuming that the injected FO frequencies are among the highest dominant oscillation modes.

Given the time derivative matrix (22) and the library matrix in (23), (21) can be obtained by a recursive threshold least-squares solution. SINDy promotes sparsity in Ξ as in (4) using an iterative Sequential Thresholded Least Squares (STLS) algorithm [35]. This approach alternates between least-squares regression and hard thresholding of small coefficients. For each state variable $k = 1, \dots, n$, the update procedure is given by (25) [35]:

$$\begin{aligned} \xi_k^{(0)T} &= \arg \min_{\xi^T} \left\| \dot{X}_k^T - \Theta(X) \xi_k^T \right\|_2^2, \\ \xi_{k,i}^{(j)} &= 0 \quad \text{if} \quad |\xi_{k,i}^{(j)}| < \lambda, \\ A_k^{(j)} &= \{i : \xi_{k,i}^{(j)} \neq 0\}, \\ \xi_k^{(j+1)T} &= \arg \min_{\xi^T \in \mathbb{R}^{|A_k^{(j)}|}} \left\| \dot{X}_k^T - \Theta(X)_{A_k^{(j)}} \xi_k^T \right\|_2^2, \end{aligned} \quad (25)$$

where ξ_k is the k -th row of Ξ , $\xi_{k,i}^{(j)}$ is the entry in row k , column i of Ξ at iteration j . $\lambda > 0$ is a sparsity threshold, and $\Theta(X)_{A_k^{(j)}}$ denotes the submatrix of active terms. This procedure is repeated until the active set $A_k^{(j)}$ stabilizes, i.e., $A_k^{(j+1)} = A_k^{(j)}$.

Looking at (21), after obtaining the estimated Ξ , the elements from its bottom left region (the shaded area in (21)), which represent the FO coefficient of angle dynamics from synchronous generators and GFL IBRs can be extracted:

$$\xi_{angle} = \begin{bmatrix} a_{\delta_1} & b_{\delta_1} & \dots & a_{\delta_l} & b_{\delta_l} \\ A_{IBR_1} & B_{IBR_1} & \dots & A_{IBR_l} & B_{IBR_l} \end{bmatrix} \quad (26)$$

Let ζ_{angle} be the square summation of the corresponding sinusoidal coefficients of the rotor angles δ and PLL output angles θ in ξ_{angle} as:

$$\zeta_{angle} = \begin{bmatrix} a_{\delta_1}^2 + b_{\delta_1}^2 & A_{IBR_1}^2 + B_{IBR_1}^2 \\ \vdots & \vdots \\ a_{\delta_l}^2 + b_{\delta_l}^2 & A_{IBR_l}^2 + B_{IBR_l}^2 \end{bmatrix} \quad (27)$$

Then, each (i, j) element in ζ_{angle} is the estimated squared magnitude of the injected FO of frequency ω_{F_i} from the generator or IBR j . Therefore, the FO frequencies ω_{F_i} and the source generators j can be identified from the highest peak values in ζ_{angle} . The proposed complete procedure for extracting the FO location is presented in Algorithm 1.

Algorithm 1: SINDy based data-driven method to locate FO in systems with IBRs

- Step 1:** Collect $\Delta\dot{\delta}$, $\Delta\dot{\theta}$, $\Delta\dot{\omega}$, and v_q measurements within a window τ_w . Compute the integral signal by (24).
 - Step 2:** Conduct an FFT analysis on measurements from each V_{ccp} . Apply the z-score-based peak detection techniques to identify the FO frequencies ω_F .
 - Step 3:** Build the time derivative matrix X (22) and the library matrix $\Theta(X)$ (23).
 - Step 4:** Obtain the coefficient matrix Ξ by (25).
 - Step 5:** Calculate ζ_{angle} by (27) and identify the sources by selecting the element with the highest peak values in ζ_{angle} .
-

Remarks:

- In **Step 1**, the method requires rotor angles and rotor speeds of synchronous generators, along with each IBR's PLL angle and Q-axis voltage component. Notably, if a bus is connected to only a single generator, PMU measurements at the CCP can be used to approximate all required values. However, when multiple generators (either synchronous generators or IBRs) are connected to the same bus, internal generator measurements are preferred for accurately locating the FO source.
- A sufficient number of measurements is necessary to be collected at **Step 1** of the proposed algorithm. In this paper, 3600 measurements are used, as the window size τ_w is 40 seconds and the sampling time is 0.017 seconds. The applied window size ensures that FO with low frequencies can be captured accurately. The two-points forward difference approximation method [33] is applied to estimate the derivatives of measurements.
- The threshold in (25) can be adjusted with respect to the number of the non-zero elements in ζ_{angle} . In this work, the threshold is selected as 0.006, allowing for three non-zero elements.
- To calculate the derivative of (22), in our case, a single differentiation does not significantly degrade numerical stability with the given sampling rate. However, in practice, engineers rarely compute derivatives directly due to noise issues of numerical differentiation, especially for higher-order derivatives or with noisy data. In practice, engineers usually use various noise mitigation strategies [36] such as smoothing before derivative (moving average, low-pass filtering), different finite-difference approximations (central, forward, backward difference), polynomial fitting (Savitzky-Golay filter, spline differentiation, etc.), and state estimation techniques (Kalman filtering, total variation regularization, etc.) [36].

- It is worth noting that the proposed method can inherently locate FO with multiple frequencies as all identified frequencies are incorporated into the feature library $\Theta(X)$. The FO sources then manifest as nonzero entries in the gray area of Ξ in (21), which SINDy utilizes for source identification. As will be elaborated in Section V-D, this makes the proposed approach advantageous with respect to existing FO locating methods that handle FO from one frequency, e.g., the VMD-CPSD method [15] and the DEF method [37].

V. NUMERICAL RESULTS

To test the proposed algorithm in an extensive system that includes both GFL IBRs and synchronous generators, a set of simulations is carried out on the WECC 240-bus test system developed by National Renewable Energy Laboratory (NREL) [16] using the commercially available TSAT software [38]. All synchronous generators are modeled with the sixth-order machine model "GENROU" equipped with exciters and turbines as presented in [38]. The generator connected to bus 1032 has been selected as the reference generator. To integrate IBRs, a Voltage Source Converter (VSC)-HVDC connection between buses 4010 and 2619 is considered which consists of the current limiter, PLL, internal voltage calculation, and outer loop control. Following Algorithm 1, measurements from both synchronous generators and GFL IBRs are used. Specifically, 24 buses with synchronous generators are selected as the monitored buses for generator rotor angle and speed measurements. The outputs of the PLL, θ and the Q-axis voltage v_q , are measured and v_{qI} is calculated by the trapezoid rule (24). In addition, there are 9 renewable generation sources including solar generation at Buses 2438, 3933, 4031, 5032, 6533, 7032 and wind generation at Buses 4031, 5032, 6533. An illustration of the monitored system is shown in Fig. 5.

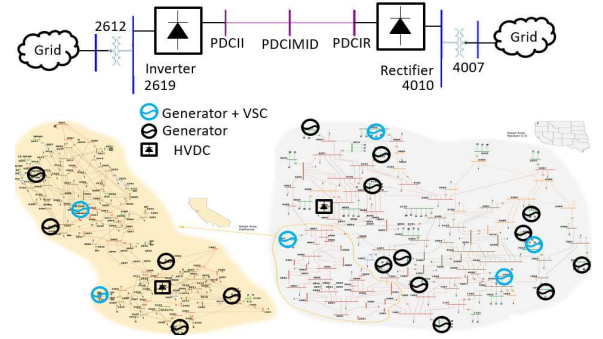


Fig. 5: Voltage Source Based Interface model [38].

A. Methods for comparison

The proposed method is validated and compared to other methods. In particular, the VMD-CPSD method presented in [15] and the DEF algorithm developed in [37] for FO locating are also implemented in TSAT for comparison.

Briefly, the VMD-CPSD method [15] exploits a cross-power spectral density analysis, focusing on the relationships between voltage magnitude and real/reactive power (SVmP / SVmQ), as well as voltage angle and real power (SVaP). It pinpoints

the FO source location based on the largest positive imaginary part of the cross-power spectral density. The DEF method [37] leverages the concept of energy dissipation within the system. Considering that in a stable power system oscillation energy should dissipate over time, DEF identifies the source of a FO by focusing on the buses where an energy amplification is observed, implying the existence of external forcing.

B. Locating Forced Oscillations from Renewable Generations

To simulate FO originating from renewable generation, a forced signal is applied to the active power control P_{ref} of various renewable converters at frequencies that coincide with the system's inter-area modes, specifically 0.379 Hz, 0.614 Hz, and 1.27 Hz, thereby creating resonance conditions. A total of 27 tests were conducted by injecting FO into each monitored renewable generator at different frequencies. Tables I, II, and III present the results for all cases. It can be observed that the proposed method successfully locates the FO source in all cases. However, the DEF and VMD-CPSD may fail to properly identify the FO source. Three such cases are highlighted in grey colors, where the DEF and VMD-CPSD methods either identify a nearby bus to the true source (light grey) or a more distant bus (dark grey). Hence, the proposed method outperforms DEF and VMD-CPSD in properly locating the FO sources from wind or solar generation.

TABLE I: Forced oscillation cases at 0.379 Hz originating from solar/wind generation

Simulation setup			DEF	SINDy	VMD-CPSD
#	FO Freq	Injection bus	Est bus	Est bus	Est bus
1	0.379Hz	6533 solar	6533	6533	6533
2		7032 solar	7032	7032	7032
3		5032 solar	5032	5032	5032
4		4031 solar	4031	4031	4031
5		3933 solar	3933	3933	3933
6		2438 solar	2438	2438	2438
7		4031 wind	4031	4031	4031
8		5032 wind	4031	5032	5032
9		6533 wind	6533	6533	6533

TABLE II: Forced oscillation cases at 0.614 Hz originating from solar/wind generation

Simulation setup			DEF	SINDy	VMD-CPSD
#	FO Freq	Injection bus	Est bus	Est bus	Est bus
1	0.614Hz	6533 solar	6533	6533	6333
2		7032 solar	7032	7032	7032
3		5032 solar	5032	5032	5032
4		4031 solar	4031	4031	4031
5		3933 solar	3933	3933	3933
6		2438 solar	2619	2438	2438
7		4031 wind	4031	4031	4031
8		5032 wind	5032	5032	5032
9		6533 wind	6533	6533	6533

To further illustrate this result, we first consider Case 8 in Table I, where the FO is injected to the active power control reference of the wind generation at Bus 5032. The V_{ccp} magnitude and angle trajectories are shown in Fig. 6 (a)

TABLE III: Forced oscillation cases at 1.27 Hz originating from solar/wind generation

Simulation setup			DEF	SINDy	VMD-CPSD
#	FO Freq	Injection bus	Est bus	Est bus	Est bus
1	1.27Hz	6533 solar	6533	6533	6533
2		7032 solar	7032	7032	7031
3		5032 solar	5032	5032	5032
4		4031 solar	4031	4031	4031
5		3933 solar	3933	3933	3933
6		2438 solar	2438	2438	2438
7		4031 wind	4031	4031	4031
8		5032 wind	5032	5032	5032
9		6533 wind	6533	6533	6533

and (b). In addition, the single-sided spectrum from FFT and the associated peak detection observation [34] are presented in Fig.6 (c) and (d). Fig. 6 indicates that the oscillation strength is 2.22% of the reference value and the frequency is 0.379 Hz. It is worth noting that despite the fact that the maximum oscillation amplitude is not at the source, the proposed algorithm can properly find the correct source location. As shown in Fig. 7 (a), this can be achieved by utilizing the rotor angle, speed, and PLL signal from the buses where renewable generation and the HVDC system are located.

Fig. 7 (b) shows that the VMD-CPSD method successfully identifies the source based on the maximum imaginary parts in SVMp quantities at the FO frequency. However, as illustrated in Fig. 7 (c), the source of the FO is misidentified by the DEF method, as the dissipate energy for bus 4031 increases whereas the FO is injected at bus 5032.

Then, we focus on Case 1 in Table II, which corresponds to injecting FO at the outer loop active power control of the solar generation at bus 6533. From Fig. 8, it can be observed that the proposed method and the DEF method can identify the true location of the FO source. Yet, the VMD-CPSD method fails to do so since the corresponding metric falsely indicates the nearby bus 6333 as the FO source.

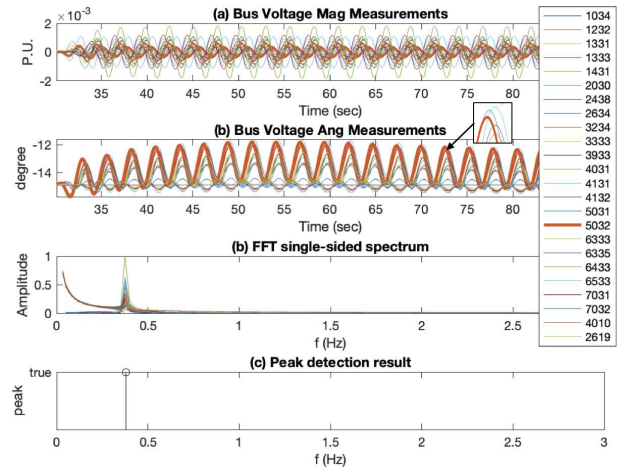


Fig. 6: (a) V_{ccp} magnitude (b) V_{ccp} angle (c) The single-sided spectrum from FFT (d) Peak frequency detection in the case of forced oscillations originating from wind generation at bus 5032.

C. Forced Oscillations due to Mistuned Controller Parameters

To test the performance of the proposed method in the case of FO due to mistuned parameters in the IBR-related controllers, FO of 0.614 Hz are injected to the VSC-HVDC converter models, specifically at the sending end bus 4010 and the receiving end bus 2619. It should be highlighted that HVDC is used instead of renewable generators because TSAT provides access to their inner loop control through a user-defined HVDC model, whereas the inner loop control of renewable generators is not accessible. As summarized in Table IV, the VMD-CPSD method is the most effective in identifying the source of FO related to HVDC converter control. While the proposed SINDy method can determine that the HVDC system is the source, it may not accurately distinguish whether the source is the sending or receiving end. In contrast, DEF often identifies nearby buses around the HVDC converter as the FO sources rather than pinpointing the actual location.

In particular, we look at Case 8 in Table IV, where the FO is injected to the inner loop D-axis current reference of bus 4010. The V_{ccp} magnitude and angle trajectories are shown in Fig. 9 (a) and (b). In addition, the single-sided spectrum from FFT and the associated peak detection observation are also shown in Fig. 9 (c) and (d).

Fig. 10 illustrates the results of the proposed method in comparison with other methods for this case. The VMD-CPSD method successfully identifies the true source of the oscillation, the sending end bus 4010 of the HVDC, as shown in Fig. 10 (b). However, while it correctly narrows the source down to the HVDC system, the proposed method mistakenly identifies the receiving end bus 2619 as the source. In contrast, the DEF method fails to identify the HVDC as the source at all, as shown in Fig. 10 (a) and (c).

In general, the results in Table IV demonstrate that the proposed method tends to misidentify the receiving end bus 2619 as the FO source rather than the sending end bus 4010. It appears that the V_{ccp} at the sending end is less sensitive compared to the V_{ccp} at the receiving end when FO stem

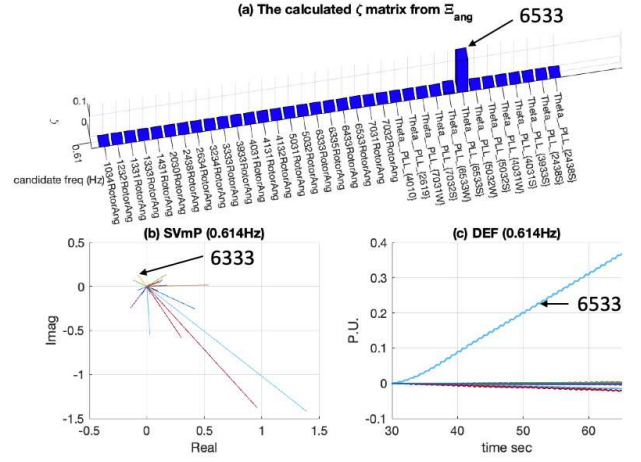


Fig. 8: (a) Proposed method (b) VMD-CPSD method (c) DEF method in the case of forced oscillations originating from solar generation at bus 6533.

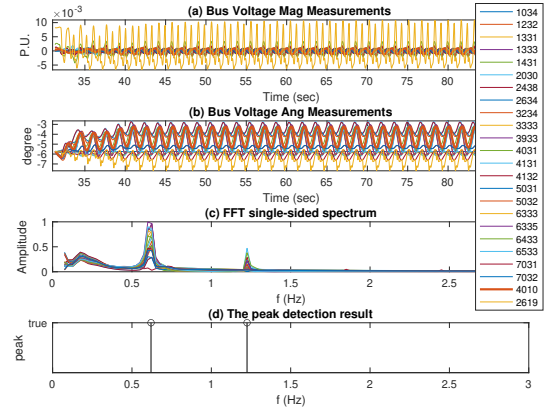


Fig. 9: (a) V_{ccp} magnitude (b) V_{ccp} angle (c) The single-sided spectrum from FFT (d) Peak frequency detection in the case of forced oscillations originating from the HVDC converter inner loop D-axis current reference at bus 4010.

from HVDC converter control. Further research is required to better understand HVDC dynamics and improve the proposed method for accurately identifying oscillations within HVDC systems.

D. Validation under Non-Stationary Forced Oscillations

A non-stationary FO event caused by renewable generation has an impact on the electromechanical modes of the system [39]. To test the performance of the proposed method when the forcing frequency and magnitude change over time, simulations are conducted with FO of multiple frequency components injected into the outer loop of the active power control of renewable generation. The oscillations are injected every 5 seconds at a single frequency selected among the resonant frequencies of 0.379 Hz, 0.614 Hz, and 1.27 Hz and with peak strengths of 1.2%, 2.22%, and 5.22% of the corresponding active power reference. Consequently, within the 40-second

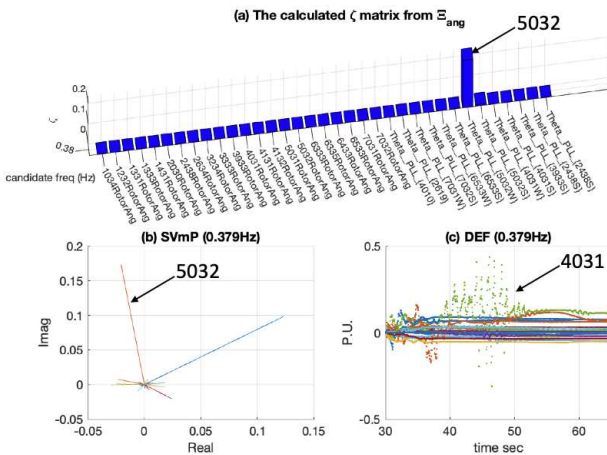


Fig. 7: (a) Proposed method (b) VMD-CPSD method (c) DEF method in the case of forced oscillations originating from wind generation at bus 5032.

TABLE IV: Forced oscillation cases originating from HVDC system

Source from HVDC system		DEF Result	SINDy Result	VMD-CPSD Result
#	Location	Est bus	Est bus	Est bus
1	2619 outer loop real power control	2619	2619	2619
2	2619 inner loop Q-axis current reference	2438	2619	2619
3	2619 inner loop D-axis current reference	2619	2619	2619
4	2619 PLL output angle	2619	4010	4010
5	4010 outer loop DC voltage control	4131	4010	4010
6	4010 outer loop AC voltage control	2619	2619	4010
7	4010 inner loop Q-axis current reference	2619	2619	4010
8	4010 inner loop D-axis current reference	1331	2619	4010
9	4010 PLL output angle	4010	4010	4010

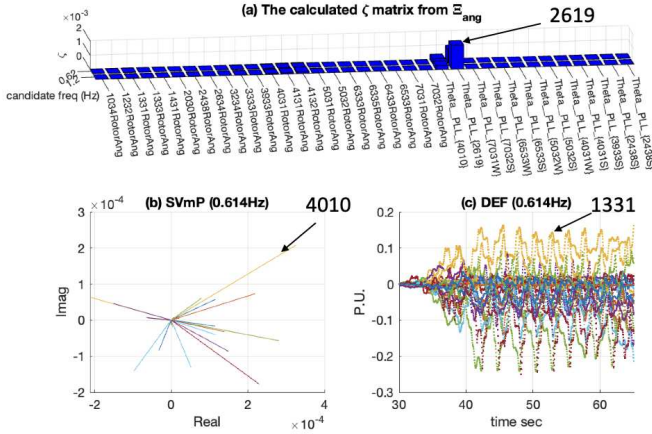


Fig. 10: (a) Proposed method (b) VMD-CPSD method (c) DEF method in the case of forced oscillations originating from the HVDC converter inner loop D-axis current reference at bus 4010.

window used by SINDy, the system experiences FO with mixed frequencies and magnitudes.

The V_{ccp} angle and magnitude trajectories in the case where non-stationary FO originates from solar generation at bus 3933 are presented in Fig. 11 (a) and (b). The corresponding single-sided spectrum from FFT and peak detection are shown in Fig. 11 (c) and (d). From Fig. 11 (c), we select three of the highest amplitude frequencies, namely, 0.725 Hz, 0.525 Hz, and 0.675 Hz, which however, are different from the true FO frequencies. Fig. 12 (a) and (b) illustrate that the proposed method and the DEF method can still correctly identify that there is FO sourced at bus 3933. In contrast, the VMD-CPSD method fails to identify the true source when using the incorrect frequencies 0.725 Hz, 0.525 Hz, and 0.675 Hz, since the corresponding highest imaginary parts do not belong to bus 3933, as shown in Fig. 12 (c) to (e). On the other hand, if the correct FO frequencies can be identified, Fig. 12 (f) validates that the VMD-CPSD method successfully locates the source when one of the true oscillation frequencies 1.27 Hz is used.

To further study the effect of non-stationary FO of varying frequencies injected in different locations, Table V provides the source locating results when using two of the true oscillation frequencies, specifically 1.27 Hz and 0.379 Hz. The simulation results suggest that the proposed SINDy method can accurately capture the true FO source whereas the other

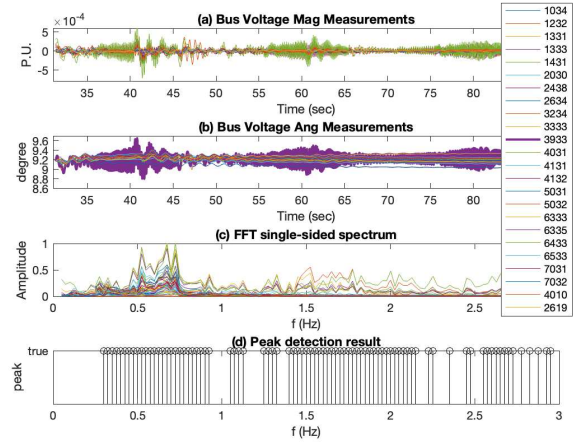


Fig. 11: (a) V_{ccp} magnitude (b) V_{ccp} angle (c) The single-sided spectrum from FFT (d) Peak frequency detection in the case of non-stationary forced oscillations originating from solar generation at Bus 3933.

two methods may fail or render inconsistent results even when true FO frequencies are applied.

For example, we consider Case 5 in Table V where the non-stationary FO is added to the active power control reference of the solar generation at Bus 5032. From Fig. 13, it can be observed that when applying the DEF and VMD-CPSD methods using the true FO frequency of 1.27 Hz, the results can turn out incorrect. This situation highlights the challenges for the DEF and VMD-CPSD methods when varying frequencies are present, as they are designed to accommodate only one FO frequency at a time. In those situations, the proposed SINDy may complement the VMD-CPSD and DEF methods in FO locating.

E. Locating Forced Oscillations from Synchronous Generators

Previous sections have mostly focused on FO sourced from IBRs. To further validate the performance of the proposed method in systems hosting both conventional generators and IBRs, in this section we present the results for the case where the FO source is a conventional synchronous generator. A simulation of 90 seconds is carried out and all synchronous generators are modeled using a sixth-order model—the “GENROU” model in TSAT—which includes rotor angle, rotor speed,

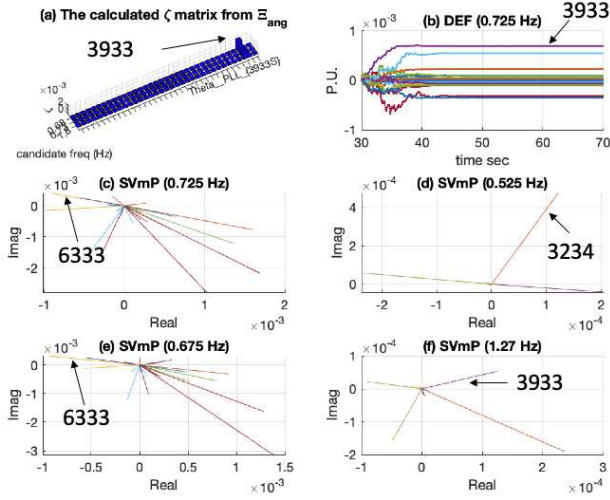


Fig. 12: (a) Proposed method (b) DEF method (c)-(f) VMD-CPSP method in the case of non-stationary forced oscillations originating from solar generation at Bus 3933.

TABLE V: Non-stationary forced oscillation cases originating from solar/wind generation

Simulation setup	DEF	SINDy	VMD-CPSP
#	Injection bus	Est at 0.379Hz	Est at 1.27Hz
1	2438 solar	2438	5031
2	3933 solar	3933	3933
3	4031 solar	4031	4031
4	4031 wind	5031	4031
5	5032 solar	5032	5031
6	5032 wind	5032	5032
7	6533 solar	6533	6533
8	6533 wind	6533	6533
9	7032 solar	7032	7032

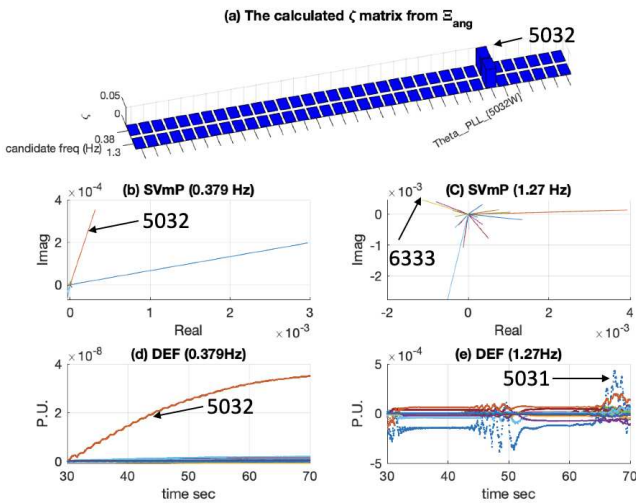


Fig. 13: (a) Proposed method (b)-(c) VMD-CPSP method (d)-(e) DEF method in the case of non-stationary forced oscillations originating from solar generation at Bus 5032.

and transient and sub-transient dynamics. Detailed excitation

systems and turbine governors are also incorporated. A forced oscillation of 1.2 Hz is injected into the active power reference of the synchronous generator on bus 2634 at 30 seconds. The FO strength is 5% of the corresponding active power reference value. All real power generations in the system experience 50db random noise (1% of the forced oscillation) as processing noise. The time window for the collection of the measurements is selected to be 40 seconds after the injection with a reporting rate of 60 frames per second. The voltage and angle trajectories of the AC bus that is immediately connected to the monitored synchronous generator rotor and the results of the FFT and peak frequency detection are presented in Fig. 14 (a)–(d).

Fig. 15 (a) shows that the proposed algorithm determines that the source is located at bus 2634 as the highest peak appears on the elements that belong to the rotor angle of the synchronous generator connected to the bus 2634 and the frequency of 1.2 Hz. This result agrees with the VMD-CPSP and DEF algorithm as shown in Fig. 15 (b) and (c).

More results can be found in Table VI, which shows the source localization results for FO injected at various generators through both exciters and governors. These results show that the proposed algorithm can successfully locate the true source location when the FO originates from conventional synchronous generators. Further supporting results can also be found in [11].

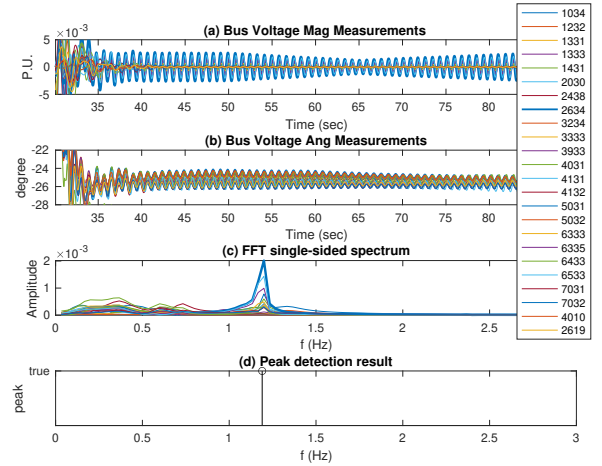


Fig. 14: (a) V_{ccp} magnitude (b) V_{ccp} angle (c) The single-sided spectrum from FFT (d) Peak frequency detection in the case of forced oscillations originating from synchronous generation at bus 2634.

TABLE VI: Forced oscillation cases with source from the synchronous generator

Simulation setup	DEF	SINDy	VMD-CPSP
#	FO Description	Inj bus	Est bus
1	Governor at 0.82 Hz	1431	1431
2	Governor at 1.19 Hz	2634	2634
3	Governor at 1.27 Hz	7031	7031
4	Exciter at 0.379 Hz	1331	1331
5	Exciter at 0.614 Hz	6333	6333

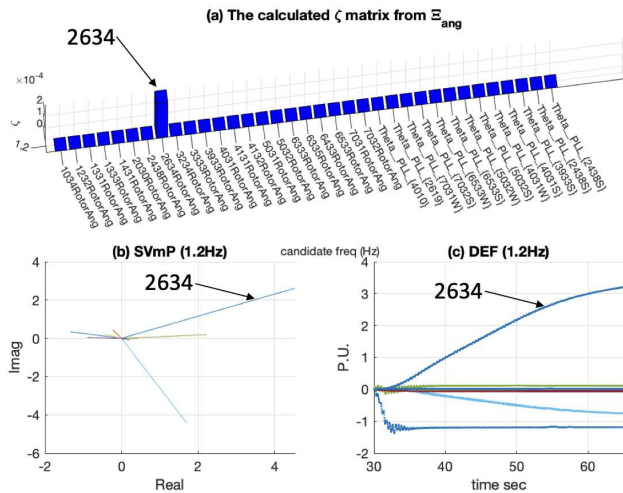


Fig. 15: (a) Proposed method (b) VMD-CPSD method (c) DEF method in the case of forced oscillations originating from synchronous generation at bus 2634.

VI. CONCLUSIONS

This paper proposes a purely data-driven algorithm for locating Forced Oscillation (FO) sources in the presence of grid-following (GFL) Inverter Based Resources (IBRs). Leveraging on Sparse Identification of Nonlinear Dynamics (SINDy), the proposed algorithm can build a linear mapping between measurements and a library filled with suitable FO source candidates including the classic generator model as well as a suitable VSC PLL dynamic model. Simulations of injecting FO in the WECC 240-bus system verify the effectiveness of the proposed algorithm in successfully locating the true FO sources under resonance conditions and non-stationary FO of various frequencies. Interestingly, it is validated that the proposed approach outperforms existing methods in the case of FO consisting of multiple frequencies. Future research will focus on further analyzing and pinpointing the location of simultaneous FO sources; how the proposed method can be extended to integrate grid-forming IBRs and their impact on system dynamics. Another promising direction is combining SINDy with physics-informed methods like DEF to improve robustness, where DEF can help regularize SINDy and mitigate its sensitivity to noise.

REFERENCES

- [1] NERC Reliability Guideline, "Forced oscillation monitoring & mitigation," Atlanta, GA, USA, 2017.
- [2] D. Watson, "Letters: Renewables caused grid a double heart attack," *The Herald*. [Online]. Available: <https://www.heraldscotland.com/news/19775696.letters-renewables-caused-grid-double-heart-attack/>
- [3] L. Chen, Y. Min, and W. Hu, "An energy-based method for location of power system oscillation source," *IEEE Transactions on Power Systems*, vol. 28, no. 2, pp. 828–836, 2012.
- [4] Y. Zhi and V. Venkatasubramanian, "Analysis of energy flow method for oscillation source location," *IEEE Transactions on Power Systems*, vol. 36, no. 2, pp. 1338–1349, 2020.
- [5] P. G. Estevez, P. Marchi, C. Galarza, and M. Elizondo, "Complex dissipating energy flow method for forced oscillation source location," *IEEE Transactions on Power Systems*, vol. 37, no. 5, pp. 4141–4144, 2022.
- [6] L. Fan, Z. Wang, Z. Miao, and S. Maslennikov, "Oscillation source detection for inverter-based resources via dissipative energy flow," *Authorea Preprints*, 2023.
- [7] B. Wang and K. Sun, "Location methods of oscillation sources in power systems: a survey," *Journal of modern power systems and clean energy*, vol. 5, no. 2, pp. 151–159, 2017.
- [8] Y. Meng, Z. Yu, N. Lu, and D. Shi, "Time series classification for locating forced oscillation sources," *IEEE Transactions on Smart Grid*, vol. 12, no. 2, pp. 1712–1721, 2021.
- [9] S. Talukder, S. Liu, H. Wang, and G. Zheng, "Low-frequency forced oscillation source location for bulk power systems: A deep learning approach," in *2021 IEEE International Conference on Systems, Man, and Cybernetics (SMC)*, 2021, pp. 3499–3404.
- [10] T. Huang, N. M. Freris, P. Kumar, and L. Xie, "A synchrophasor data-driven method for forced oscillation localization under resonance conditions," *IEEE Transactions on Power Systems*, vol. 35, no. 5, pp. 3927–3939, 2020.
- [11] Y. Cai, X. Wang, G. Joós, and I. Kamwa, "An online data-driven method to locate forced oscillation sources from power plants based on sparse identification of nonlinear dynamics (sindy)," *IEEE Transactions on Power Systems*, vol. 38, no. 3, pp. 2085–2099, 2023.
- [12] S. Feng, J. Chen, Y. Ye, X. Wu, H. Cui, Y. Tang, and J. Lei, "A two-stage deep transfer learning for localisation of forced oscillations disturbance source," *International Journal of Electrical Power & Energy Systems*, vol. 135, p. 107577, 2022. [Online]. Available: <https://www.sciencedirect.com/science/article/pii/S0142061521008115>
- [13] S. L. Brunton, J. L. Proctor, and J. N. Kutz, "Sparse identification of nonlinear dynamics with control (SINDy)," *IFAC-PapersOnLine*, vol. 49, no. 18, pp. 710–715, 2016.
- [14] K. V. S. M. Babu, P. Chakraborty, and M. Pal, "Identification of forced oscillation sources in wind farms using e-sindy," in *2023 IEEE IAS Global Conference on Emerging Technologies (GlobConET)*, 2023, pp. 1–6.
- [15] D. Osipov, S. Konstantinopoulos, and J. H. Chow, "A cross-power spectral density method for locating oscillation sources using synchrophasor measurements," *IEEE Transactions on Power Systems*, vol. 38, no. 6, pp. 5526–5534, 2023.
- [16] H. Yuan, R. S. Biswas, J. Tan, and Y. Zhang, "Developing a reduced 240-bus wecc dynamic model for frequency response study of high renewable integration," in *2020 IEEE/PES Transmission and Distribution Conference and Exposition (T&D)*. IEEE, 2020, pp. 1–5.
- [17] X. Wang, J. W. Bialek, and K. Turitsyn, "PMU-based estimation of dynamic state Jacobian matrix and dynamic system state matrix in ambient conditions," *IEEE Transactions on Power Systems*, vol. 33, no. 1, pp. 681–690, 2017.
- [18] I. Zenelis, X. Wang, and I. Kamwa, "Online PMU-Based Wide-Area Damping Control for Multiple Inter-Area Modes," *IEEE Transactions on Smart Grid*, vol. 11, no. 6, pp. 5451–5461, 2020.
- [19] Y. Gu and T. C. Green, "Power system stability with a high penetration of inverter-based resources," *Proceedings of the IEEE*, 2022.
- [20] D. S. Dolan and P. W. Lehn, "Simulation model of wind turbine 3p torque oscillations due to wind shear and tower shadow," in *2006 IEEE PES Power Systems Conference and Exposition*. IEEE, 2006, pp. 2050–2057.
- [21] Z. Chen, J. M. Guerrero, and F. Blaabjerg, "A review of the state of the art of power electronics for wind turbines," *IEEE Transactions on Power Electronics*, vol. 24, no. 8, pp. 1859–1875, 2009.
- [22] C. Su, W. Hu, Z. Chen, and Y. Hu, "Mitigation of power system oscillation caused by wind power fluctuation," *IET Renewable Power Generation*, vol. 7, no. 6, pp. 639–651, 2013. [Online]. Available: <https://ietresearch.onlinelibrary.wiley.com/doi/abs/10.1049/iet-rpg.2012.0253>
- [23] R. Inzunza, Y. Tawada, M. Furukawa, N. Shibata, T. Sumiya, T. Tanaka, and M. Kinoshita, "Behavior of a photovoltaic inverter under sudden increase in irradiance due to reflection in clouds," in *2015 International Conference on Renewable Energy Research and Applications (ICRERA)*, 2015, pp. 851–855.
- [24] I. Ranaweera, O.-M. Midtgård, and G. H. Yordanov, "Short-term intermittency of solar irradiance in southern norway," in *29th European Photovoltaic Solar Energy Conference and Exhibition (EUPVSEC)*, 2014, pp. 2635–2638.
- [25] A. Kankiewicz, M. Sengupta, and D. Moon, "Observed impacts of transient clouds on utility-scale pv fields," in *Solar 2010 Conference Proceedings*, vol. 2009, 2010.
- [26] J. A. Nelson, *Effects of cloud-induced photovoltaic power transients on power system protection*. California Polytechnic State University, 2010.

- [27] T. Surinkaew, K. Emami, R. Shah, S. Islam, and N. Mithulananthan, "Forced oscillation in power system with renewable generations," in *2020 2nd International Conference on Smart Power & Internet Energy Systems (SPIES)*. IEEE, 2020, pp. 287–292.
- [28] L. Fan, Z. Miao, D. Piper, D. Ramasubramanian, L. Zhu, and P. Mitra, "Analysis of 0.1-hz var oscillations in solar photovoltaic power plants," *IEEE Transactions on Sustainable Energy*, vol. 14, no. 1, pp. 734–737, 2022.
- [29] T. L. Vandoorn, J. De Kooning, B. Meersman, and L. Vandevelde, "Voltage-based droop control of renewables to avoid on-off oscillations caused by overvoltages," *IEEE Transactions on Power Delivery*, vol. 28, no. 2, pp. 845–854, 2013.
- [30] S. Lu, Z. Xu, L. Xiao, W. Jiang, and X. Bie, "Evaluation and enhancement of control strategies for vsc stations under weak grid strengths," *IEEE Transactions on Power Systems*, vol. 33, no. 2, pp. 1836–1847, 2017.
- [31] L. Fan, Z. Miao, and D. Ramasubramanian, "Ibr power plant frequency control design consideration," *IEEE Transactions on Sustainable Energy*, vol. 15, no. 4, pp. 2405–2416, 2024.
- [32] J. Wang, J. D. Yan, L. Jiang, and J. Zou, "Delay-dependent stability of single-loop controlled grid-connected inverters with lcl filters," *IEEE Transactions on Power Electronics*, vol. 31, no. 1, pp. 743–757, 2016.
- [33] G. Lindfield and J. Penny, *Numerical methods: using MATLAB*. Academic Press, 2018.
- [34] J. Van Brakel. "Robust peak detection algorithm using Z-scores". [Online]. Available: <https://stackoverflow.com/questions/22583391/peak-signal-detection-in-realtime-timeseries-data> (accessed December 16th)
- [35] S. L. Brunton and J. N. Kutz, *Data-driven science and engineering: Machine learning, dynamical systems, and control*. Cambridge University Press, 2019.
- [36] W. H. Press, *Numerical recipes 3rd edition: The art of scientific computing*. Cambridge university press, 2007.
- [37] S. Maslennikov and E. Litvinov, "Iso new england experience in locating the source of oscillations online," *IEEE Transactions on Power Systems*, vol. 36, no. 1, pp. 495–503, 2020.
- [38] P. Inc. Tsat transient security assessment tool model manual. [Online]. Available: <https://powertechlabs.com> (accessed November 27th 2022)
- [39] T. Surinkaew, K. Emami, R. Shah, and N. Mithulananthan, "Effects of non-stationary forced oscillation on electromechanical modes," in *2021 IEEE PES Innovative Smart Grid Technologies - Asia (ISGT Asia)*, 2021, pp. 1–5.



Yaojie Cai received the MSc degrees in electrical and computer engineering from the University of Manitoba, Winnipeg, MB, Canada. He is currently working toward the Ph.D. degree in electrical and computer engineering with McGill University, QC, Canada. His research interests include data analytics, power system stability and control.



Georgia Pierrou (Member, IEEE) received the Diploma in electrical and computer engineering from the National Technical University of Athens, Athens, Greece in 2017, and the Ph.D. degree from McGill University, Montreal, QC, Canada, in 2021. She is currently a Postdoctoral Researcher with the Power Systems Laboratory, ETH Zurich, Zurich, Switzerland. Her research interests include dynamic analysis, optimization, and control of electric power systems.



and control, uncertainty quantification in power system security, stability and resilience, and cybersecurity in power systems.

Xiaozhe Wang (Senior Member, IEEE) received the B.S. degree in information science and electronic engineering from Zhejiang University, Zhejiang, China, in 2010, and the Ph.D. degree from the School of Electrical and Computer Engineering, Cornell University, Ithaca, NY, USA, in 2015. She is currently an Associate Professor and a Canada Research Chair with the Department of Electrical and Computer Engineering, McGill University, Montreal, QC, Canada. Her research interests include data-driven power system stability monitoring



Concordia University (Montreal, Canada). He is active in IEEE Standards Association working groups on distributed energy resources and microgrids. He is a Fellow of CIGRE, and the Canadian Academy of Engineering.

Géza Joós (Life Fellow, IEEE) graduated from McGill University, Montreal, Canada, with an M.Eng. and Ph.D. in Electrical Engineering. He is a Professor in the Department of Electrical and Computer Engineering Department at McGill University (since 2001). He holds a Canada Research Chair in Powering Information Technologies (since 2004). His research interests are in distributed energy resources, including renewable energy resources, advanced distribution systems and microgrids. He was previously with ABB, the Université du Québec and